crystals

MDPI

Communication

Gap-Size-Dependent Effective Phase Transition in Metasurfaces of Closed-Ring Resonators

Seojoo Lee [1] and Ji-Hun Kang [2,3,4,*]

[1] Department of Mechanical Engineering, Korea Advanced Institute of Science and Technology (KAIST), Daejeon 34141, Korea; seojoo@kaist.ac.kr
[2] Department of Optical Engineering, Kongju National University, Cheonan 31080, Korea
[3] Department of Future Convergence Engineering, Kongju National University, Cheonan 31080, Korea
[4] Institute of Application and Fusion for Light, Kongju National University, Cheonan 31080, Korea
* Correspondence: jihunkang@kongju.ac.kr

Abstract: We theoretically investigate a metal-to-insulator transition in artificial two-dimensional (2D) crystals (i.e., metasurfaces) of tightly coupled closed-ring resonators. Strong interaction between unit resonators in the metasurfaces yields the effective permittivity highly dependent on the lattice spacing of unit resonators. Through our rigorous theory, we provide a closed form of effective permittivity of the metasurface and reveal that the permittivity possesses a Lorentzian-type resonant behavior, implying that the transition of the effective permittivity can arise when the lattice spacing passes a critical value.

Keywords: effective medium description; metasurface; metamaterials; metal-to-insulator transition

check for updates

Citation: Lee, S.; Kang, J.-H. Gap-Size-Dependent Effective Phase Transition in Metasurfaces of Closed-Ring Resonators. *Crystals* **2021**, *11*, 684. https://doi.org/10.3390/cryst11060684

Academic Editors: Behrad Koohbor and Amin Nozariasbmarz

Received: 13 April 2021
Accepted: 9 June 2021
Published: 14 June 2021

Publisher's Note: MDPI stays neutral with regard to jurisdictional claims in published maps and institutional affiliations.

Copyright: © 2021 by the authors. Licensee MDPI, Basel, Switzerland. This article is an open access article distributed under the terms and conditions of the Creative Commons Attribution (CC BY) license (https://creativecommons.org/licenses/by/4.0/).

1. Introduction

Metal-to-insulator transition is an essential physical phenomenon in crystal solids as it results in drastic changes in electrical and optical responses of materials [1–3]. In artificial crystals, such as three-dimensional metamaterials and two-dimensional metasurfaces, the notion of transition can be extended in the context of an effective medium theory. It was shown that artificial assemblies of subwavelength unit resonators can exhibit either metal or insulator phases [4,5] during light–matter interaction. Hyperbolic metasurfaces [6–8] that utilize both metal and insulator phases for separate principal axes are now at the core of various applications [9–12], realizing unprecedented optical properties. Moreover, in high-density metasurfaces, the transition is shown to be controllable by the coupling strength between unit resonators [13,14].

Likewise, owing to its importance, the metal-to-insulator transition in metasurfaces has been investigated in various structures. However, despite such extensive studies, detailed physical accounts (i.e., physical interpretations of the effective phase and the transition condition) have not been intensively made yet. More importantly, understanding of the underlying physics of the phase transition is still desired to capture an intuitive picture of the transition and for further development of relevant applications. In this paper, we consider metasurfaces with tightly coupled resonators and show that the metal-to-insulator transition arises in metasurfaces depending on the strength of coupling. In particular, we make a rigorous analysis on a model metasurface composed of closed-ring unit resonators and provide accurate and physically intuitive criteria for the transition. When resonators are capacitively coupled to each other with a deep subwavelength lattice spacing, we find that the metal-to-insulator transition occurs when the lattice spacing exceeds a critical value. We also clarify the underlying physical mechanism of the phase transition in terms of light transmission in metasurfaces through two competing transmission channels.

2. Theoretical Model

The phase of a metasurface can be expressed in terms of its effective permittivity and permeability. These effective parameters are governed by the interaction of light with constituent resonator elements. For tightly coupled resonators, the conventional effective medium approaches used with dilute metasurfaces, such as the Maxwell Garnett theory, do not apply [15]. Here, we make a rigorous coupled-mode theory calculation to derive effective parameters for dense metasurfaces. Consider an exemplary metasurface composed of subwavelength rectangular ring resonators, as shown in Figure 1. Resonators are spaced periodically with gap sizes g_x and g_y in the x- and y-directions.

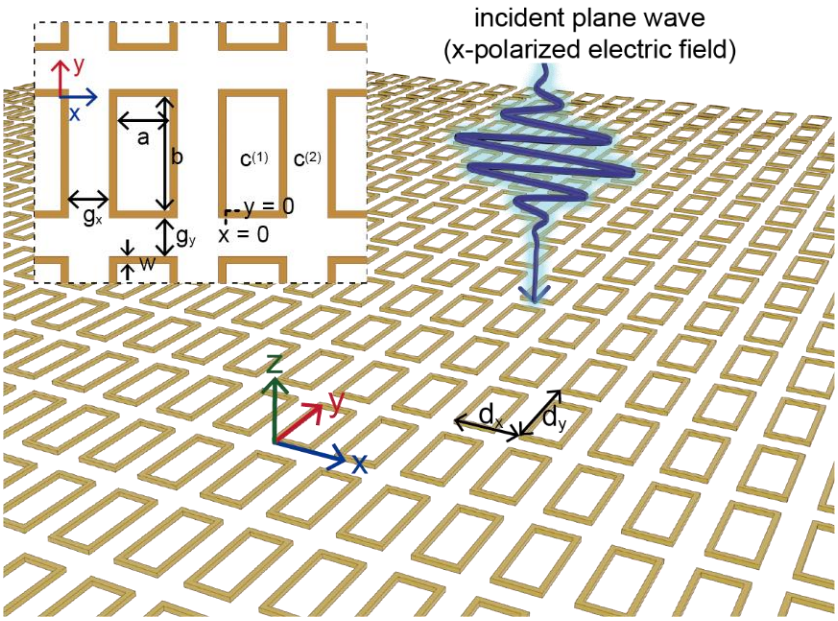

Figure 1. Schematic of a metasurface consisting of rectangular closed-ring resonators of perfect electric conductors. The incident is an x-polarized plane wave impinging upon the metasurface normally. $c^{(1)}$ and $c^{(2)}$ denote the two dominant light channels in the metasurface.

To simplify the problem, we assume that the rectangular rings are made of a perfect electric conductor (PEC) with side lengths a, b ($a < b$) smaller than the wavelength λ of the incident light. For tightly coupled resonators with narrow gaps g_x, $g_y \ll \lambda$, nearby resonators can interact with each other through charges induced by incident light [16]. These capacitive interactions open a highly efficient transmission channel through the gap (channel $c^{(2)}$) mediated by the funneling process [17,18]. Together with the channel $c^{(1)}$ through the open rectangular hole region, the gap channel $c^{(2)}$ determines the phase of the metasurface. To determine the transition analytically, we adopt the coupled-mode theory [19,20]. For an x-polarized electric field incident normally onto the metasurface (region II, $-h/2 < z < h/2$) as illustrated in Figure 1, magnetic fields in regions I ($z < -h/2$) and III ($z > h/2$) can be expanded in terms of quantized diffracted waves of orders m and n:

$$\begin{aligned} \vec{H}_I &= Z_0^{-1}\left[\hat{y}e^{ik_0(z+\frac{h}{2})} + \sum_{m,n=-\infty}^{\infty} \vec{R}_{mn} e^{-i\chi_{mn}(z+\frac{h}{2})+i\phi_{mn}}\right] \\ \vec{H}_{III} &= Z_0^{-1} \sum_{m,n=-\infty}^{\infty} \vec{T}_{mn} e^{i\chi_{mn}(z-\frac{h}{2})+i\phi_{mn}}, \end{aligned} \tag{1}$$

where $Z_0 \equiv (\mu_0/\varepsilon_0)^{1/2}$ is the free-space impedance, $\varphi_{mn} \equiv \alpha_m(x - a/2) + \beta_n(y - b/2)$, $\alpha_m \equiv 2\pi m/d_x$, $\beta_n \equiv 2\pi n/d_y$, $\chi_{mn} \equiv \left(k_0^2 - \alpha_m^2 - \beta_n^2\right)^{1/2}$, and $k_0 \equiv 2\pi/\lambda$. Inside the metasurface region II, we treat the rectangular hole region and gap region separately. In the gap region, we note that the x-polarized electric field barely couples to the gap region parallel

to the x-axis ($-w < x < a + w$, $b + w < y < b + w + g_y$) due to the strong cut-off condition. Subsequently, we neglect electromagnetic (EM) waves inside this gap region and consider only the remaining gap $c^{(2)}$ ($a + w \le x \le a + w + g_x$). In the rectangular region $c^{(1)}$ ($0 \le x \le a$, $0 \le y \le b$), we make a single-mode approximation and consider only the fundamental waveguide mode [20]. This allows for writing the EM waves inside the metasurface as

$$\vec{E}_{II}^{(1)} = \left(\sin\left(\frac{\pi y}{b}\right)\left(A_1 e^{ik_1 z} + B_1 e^{-ik_1 z}\right), 0, 0\right), \ \vec{H}_{II}^{(2)} = \left(0, Z_0^{-1}\left(A_2 e^{ik_0 z} + B_0 e^{-ik_0 z}\right), 0\right), \tag{2}$$

with $k_1 \equiv \left(k_0^2 - \pi^2/b^2\right)^{1/2}$. The remaining field components can be obtained from Maxwell's equations. By applying continuity boundary conditions of tangential EM fields at two interfaces $z = \pm h/2$, all the undetermined coefficients A_j, B_j, $\vec{T}_{mn} \equiv \left(T_{x,mn}, T_{y,mn}, T_{z,mn}\right)$, and $\vec{R}_{mn} \equiv \left(R_{x,mn}, R_{y,mn}, R_{z,mn}\right)$ can be fixed. Specifically, one can readily show that the continuity of E_y at two interfaces ($z = \pm h/2$) and the divergencelessness of the magnetic field give constraints such that [20]

$$\begin{aligned} R_{x,mn} &= -\tfrac{\alpha_m \beta_n}{\alpha_m^2 + \chi_{mn}^2} R_{y,mn}, \ R_{z,mn} = \tfrac{\beta_n \chi_{mn}}{\alpha_m^2 + \chi_{mn}^2} R_{y,mn}, \\ T_{x,mn} &= -\tfrac{\alpha_m \beta_n}{\alpha_m^2 + \chi_{mn}^2} T_{y,mn}, \ T_{z,mn} = -\tfrac{\beta_n \chi_{mn}}{\alpha_m^2 + \chi_{mn}^2} T_{y,mn}. \end{aligned} \tag{3}$$

Then, the continuity conditions of E_x at two interfaces can be simplified as

$$\begin{aligned} 1 - \sum_{m,n=-\infty}^{\infty}\left(\tfrac{k_0 \chi_{mn}}{\alpha_m^2 + \chi_{mn}^2} R_{y,mn} e^{i\phi_{mn}}\right) &= \sin\left(\tfrac{\pi y}{b}\right)\left(A_1 e^{-ik_1 h/2} + B_1 e^{ik_1 h/2}\right) && (\text{on } c^{(1)}) \\ &= A_2 e^{-ik_0 h/2} + B_2 e^{ik_0 h/2} && (\text{on } c^{(2)}) \\ &= 0 && (\text{otherwise}), \end{aligned} \tag{4}$$

and

$$\begin{aligned} \sum_{m,n=-\infty}^{\infty}\left(\tfrac{k_0 \chi_{mn}}{\alpha_m^2 + \chi_{mn}^2} T_{y,mn} e^{i\phi_{mn}}\right) &= \sin\left(\tfrac{\pi y}{b}\right)\left(A_1 e^{ik_1 h/2} + B_1 e^{-ik_1 h/2}\right) && (\text{on } c^{(1)}) \\ &= A_2 e^{ik_0 h/2} + B_2 e^{-ik_0 h/2} && (\text{on } c^{(2)}) \\ &= 0 && (\text{otherwise}). \end{aligned} \tag{5}$$

Now, the inverse Fourier transform of Equations (4) and (5) gives rise to

$$\begin{aligned} \delta_{m0}\delta_{n0} - \tfrac{k_0 \chi_{mn}}{\alpha_m^2 + \chi_{mn}^2} R_{y,mn} &= Q_{mn}\left[A_1 e^{-ik_1 h/2} + B_1 e^{ik_1 h/2}\right] + \widetilde{Q}_{mn}\left[A_2 e^{-ik_0 h/2} + B_2 e^{ik_0 h/2}\right], \\ \tfrac{k_0 \chi_{mn}}{\alpha_m^2 + \chi_{mn}^2} T_{y,mn} &= Q_{mn}\left[A_1 e^{ik_1 h/2} + B_1 e^{-ik_1 h/2}\right] + \widetilde{Q}_{mn}\left[A_2 e^{ik_0 h/2} + B_2 e^{-ik_0 h/2}\right]. \end{aligned} \tag{6}$$

Here, δ_{mn} is the Kronecker delta. Q_{mn} and $\widetilde{Q}_{mn}$ are vector dependencies between external diffracted waves and internal waveguide modes in two channels, and are defined as

$$Q_{mn} \equiv \frac{1}{d_x d_y}\int_0^a \int_0^b dxdy \sin\left(\frac{\pi y}{b}\right) e^{-i\phi_{mn}}, \ \widetilde{Q}_{mn} \equiv \frac{1}{d_x d_y}\int_{a+w}^{a+w+g_x} \int_0^{d_y} dxdy e^{-i\phi_{mn}}. \tag{7}$$

Equation (6) gives the relationship between the waveguide modes in the metasurface and the diffracted waves in the free space. In particular, we note that the zero-th order transmission and reflection coefficients can be written as

$$\begin{aligned} T_{y,00} &= \tfrac{2ab}{d_x d_y \pi}\left[A_1 e^{ik_1 h/2} + B_1 e^{-ik_1 h/2}\right] + \tfrac{g_x}{d_x}\left[A_2 e^{ik_0 h/2} + B_2 e^{-ik_0 h/2}\right], \\ R_{y,00} &= 1 - \tfrac{2ab}{d_x d_y \pi}\left[A_1 e^{-ik_1 h/2} + B_1 e^{ik_1 h/2}\right] - \tfrac{g_x}{d_x}\left[A_2 e^{-ik_0 h/2} + B_2 e^{ik_0 h/2}\right]. \end{aligned} \tag{8}$$

The results so far are obtained from the continuity of the tangential components of the electric fields at two interfaces. In order to fix the undetermined coefficients $A_{1,2}$ and

$B_{1,2}$, the same procedure can be applied to the continuity of the magnetic fields. After a straightforward calculation, one can find that $A_{1,2}$ and $B_{1,2}$ can be obtained from a matrix equation $C = M^{-1}G$, where a 4×4 matrix M is defined by

$$M \equiv \begin{pmatrix} e^{-ik_1\frac{h}{2}}\left(W_{1,1}+\frac{k_1}{k_0}\right) & e^{ik_1\frac{h}{2}}\left(W_{1,1}-\frac{k_1}{k_0}\right) & e^{-ik_0\frac{h}{2}}W_{1,2} & e^{ik_0\frac{h}{2}}W_{1,2} \\ e^{ik_1\frac{h}{2}}\left(W_{1,1}-\frac{k_1}{k_0}\right) & e^{-ik_1\frac{h}{2}}\left(W_{1,1}+\frac{k_1}{k_0}\right) & e^{ik_0\frac{h}{2}}W_{1,2} & e^{-ik_0\frac{h}{2}}W_{1,2} \\ e^{-ik_1\frac{h}{2}}W_{2,1} & e^{ik_1\frac{h}{2}}W_{2,1} & e^{-ik_0\frac{h}{2}}(W_{2,2}+1) & e^{ik_0\frac{h}{2}}(W_{2,2}-1) \\ e^{-ik_1\frac{h}{2}}W_{2,1} & e^{-ik_1\frac{h}{2}}W_{2,1} & e^{ik_0\frac{h}{2}}(W_{2,2}-1) & e^{-ik_0\frac{h}{2}}(W_{2,2}+1) \end{pmatrix}, \quad (9)$$

with two column vectors $C^{\mathrm{T}} \equiv (A_1, B_1, A_2, B_2)$ and $G^{\mathrm{T}} \equiv (\pi/8, 0, 2, 0)$, where $^{\mathrm{T}}$ denotes the transpose. $W_{j,l}$ is the light-channel coupling factor given by

$$W_{j,l} \equiv \frac{2-\delta_{j2}}{S\left(c^{(j)}\right)d_x d_y}\sum_{m,n=-\infty}^{\infty}\frac{\alpha_m^2+\chi_{mn}^2}{k_0\chi_{mn}}\left(\int_{c^{(j)}}dxdyu_y^{(j)}e^{i\phi_{mn}}\right)\left(\int_{c^{(l)}}dxdyu_y^{(l)}e^{-i\phi_{mn}}\right). \quad (10)$$

Here, $S(c^{(j)})$ is the cross-sectional area of the channel $c^{(j)}$ in the $x-y$ plane, and $u_y^{(1)} \equiv \sin(\pi y/b)$ and $u_y^{(2)} \equiv 1$ are the waveguide mode profile. When the ring resonators are in a deep subwavelength scale, the coupling factors can be approximately written as

$$\begin{aligned} &W_{1,1} \approx \tfrac{8ab}{\pi^2 d_x d_y} + i\tfrac{4ad_y^2}{k_0\pi b^3 d_x},\ W_{2,2} \approx g_x\left(\tfrac{1}{d_x} + i\tfrac{k_0}{\pi}\Omega\right), \\ &W_{1,2} \approx \tfrac{4g_x}{\pi d_x} - ig_x^2\tfrac{4k_0}{a\pi^2}\widetilde{\Omega},\ W_{2,1} \approx \tfrac{2ab}{\pi d_x d_y} - ig_x\tfrac{2k_0 b}{\pi^2 d_y}\widetilde{\Omega}, \end{aligned} \quad (11)$$

where

$$\begin{aligned} &\Omega \equiv \ln\left(\tfrac{2g_x\pi}{d_x}\right) - \tfrac{3}{2}, \\ &\widetilde{\Omega} \equiv \left[\ln\left(\tfrac{2\pi(w+g_x)}{d_x}\right) + \tfrac{2w}{g_x}\ln\left(\tfrac{2\pi(w+g_x)}{d_x}\right) + \tfrac{w^2}{g_x^2}\ln\left(\tfrac{w+g_x}{w}\right) - \tfrac{3w}{g_x} - \tfrac{3}{2}\right]. \end{aligned} \quad (12)$$

The deep subwavelength thickness of the metasurface allows for approximating Equation (9). By expanding up to linear terms of $k_0 h$ and $k_1 h$, we finally arrive at simplified zero-th order transmission and reflection coefficients that are necessary to define the effective parameters:

$$\begin{aligned} &T_{y,00} \approx F + i\sigma, R_{y,00} \approx 1 - F + i\sigma, \\ &F \equiv \tfrac{1}{\pi\eta}\left[\tfrac{2ab}{d_x d_y \pi}(-\pi W_{1,2} + 4W_{2,2} - 2ik_0 h) + \tfrac{g_x}{d_x}\left(\pi W_{1,1} - i\pi\tfrac{k_1^2 h}{2k_0} - 4W_{2,1}\right)\right], \\ &\sigma \equiv k_0 h\left(\tfrac{4ab}{d_x d_y \pi^2} + \tfrac{g_x}{2d_x}\right),\ \eta \approx W_{1,1}W_{2,2} - iW_{1,1}\tfrac{k_0 h}{2} - iW_{2,2}\tfrac{k_1^2 h}{2k_0} - W_{1,2}W_{2,1}. \end{aligned} \quad (13)$$

3. Retrieval of Effective Indices of the Metasurface from Transmission and Reflection Coefficients

The main idea of defining the effective indices is to replace the inhomogeneous structures by unstructured homogeneous media by keeping the scattering properties unchanged. Since the near and far fields in unstructured media are exactly the same, the homogenization is usually done by matching the far-field scattering properties, which is valid only for the structures having subwavelength periodicity. The retrieval methods of effective indices are introduced in various literatures. Here, we follow the scheme present in [21]. In terms of transmission and reflection coefficients, T and R, the effective refractive index and impedance can be written as [21].

$$n_{eff} = \frac{1}{k_0 h}\arccos\left(\frac{1+T^2-R^2}{2T}\right),\ Z_{eff} = \sqrt{\frac{(1-R^2)^2-T^2}{(1+R^2)^2-T^2}}. \tag{14}$$

Since we assume that the metasurface is made of PEC and the lattice constant is smaller than the incident wavelength, the system is lossless, and only zero-th order diffracting waves can reach the far field. We note that this constraint allows a further simplification of Equation (14). One can readily show that the transmission and reflection coefficients in the complex plane are orthogonal to each other when the media are lossless:

$$\mathrm{Re}(T)\mathrm{Re}(R) + \mathrm{Im}(T)\mathrm{Im}(R) = 0. \tag{15}$$

Together with energy conservation, $|T|^2 + |R|^2 = 1$, one can find that the relation $\left(1+T^2-R^2\right)/2T = \mathrm{Re}(T)/|T|^2$ holds. Consequently, Equation (14) can be reduced as

$$n_{eff} = \frac{1}{k_0 h}\arccos\left(\frac{\mathrm{Re}(T)}{|T|^2}\right),\ Z_{eff} = \sqrt{\frac{\mathrm{Re}(R)-|R|^2}{\mathrm{Re}(R)+|R|^2}}. \tag{16}$$

Replacing T and R in Equation (16) with $T_{y,00}$ and $R_{y,00}$ yields the effective index and impedance of the metasurface. For instance, let us examine the refractive index. By putting Equation (13) into $\left|T_{y,00}\right|_2 + \left|R_{y,00}\right|_2 = 1$, one can find that $\left|T_{y,00}\right|^2$ can be approximated as $\mathrm{Re}(F) + 2\mathrm{Im}(F)\sigma$. This gives a significantly simplified form of the refractive index:

$$\begin{aligned} n_{eff} &= \tfrac{1}{k_0 h}\arccos\left(\tfrac{\mathrm{Re}\left(T_{y,00}\right)}{\left|T_{y,00}\right|^2}\right) \approx \tfrac{1}{k_0 h}\arccos\left(\tfrac{\mathrm{Re}(F)}{\mathrm{Re}(F)+2\mathrm{Im}(F)\sigma}\right) \\ &= \tfrac{1}{k_0 h}\arccos\left(1-\tfrac{2\mathrm{Im}(F)\sigma}{\mathrm{Re}(F)+2\mathrm{Im}(F)\sigma}\right) = \tfrac{1}{k_0 h}\arccos\left(1-\tfrac{2\mathrm{Re}(\eta)\sigma}{\mathrm{Im}(\eta)+2\mathrm{Re}(\eta)\sigma}\right). \end{aligned} \tag{17}$$

In the last step in Equation (17), we used the fact that $\mathrm{Re}(-\pi W_{1,2} + 4W_{2,2}) = 0$ and $\mathrm{Re}(\pi W_{1,1} - 4W_{2,1}) = 0$ from Equations (11) and (13). Note that σ is real-valued and very small when $h, g_x \ll a, b$. Equations (16) and (17) clearly show that there is a singularity at $T_{y,00} = 0 = \mathrm{Re}(F) + 2\mathrm{Im}(F)\sigma$. One can find that this singularity corresponds to the transition point at which the effective refractive indices change from real (imaginary) to imaginary (real), and that the absolute value of $\mathrm{Im}(F)\sigma/(\mathrm{Re}(F) + 2\mathrm{Im}(F)\sigma)$ is always smaller than 1 except when it is very close to the singularity. This allows for approximating Equation (17) such that

$$n_{eff} \approx \frac{1}{k_0 h}\sqrt{\frac{4\mathrm{Re}(\eta)\sigma}{\mathrm{Im}(\eta)+2\mathrm{Re}(\eta)\sigma}}\left(1+O\left(\sigma^2\right)+\ldots\right). \tag{18}$$

The validity of this approximation is shown in Figure 2. However, note that Equation (18) holds the same singularity with Equation (17), implying that the transition condition in Equation (17) is still valid in Equation (18). By putting all geometric parameters in Equations (11) and (13) into Equation (18) and keeping up to the linear terms of g_x/Γ and h/Γ, where Γ is one of all other geometric parameters much larger than g_x and h, we arrive at

$$n_{eff} \approx \sqrt{\frac{8ad_y^2}{hk_0^2 d_x b^3 \pi}}\sqrt{\frac{\Omega - \pi h/2g_x}{\pi h/2g_x - \Omega - \pi^2 d_y^3/k_0^2 b^4 d_x}}. \tag{19}$$

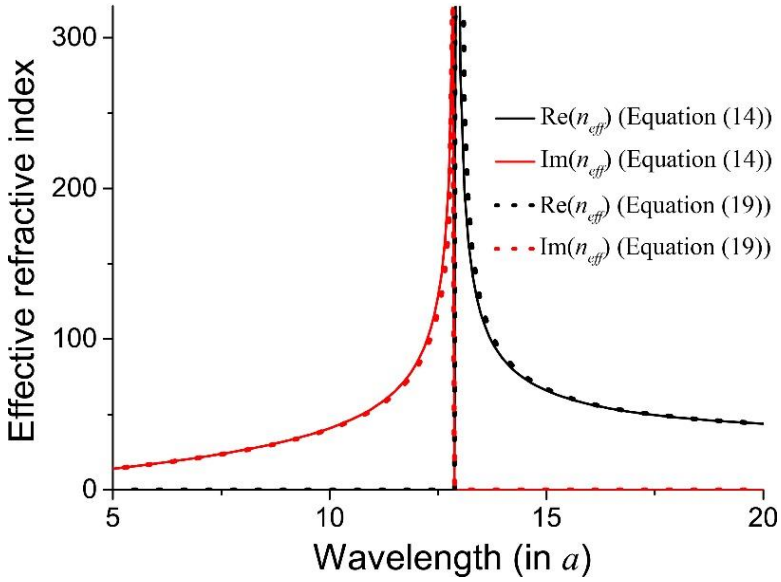

Figure 2. Comparison of exact and approximated effective refractive indices calculated from Equations (14) and (19), respectively. Here, we set $a = b$, $d_x = d_y = 1.021a$, $g_x = g_y = 0.001a$, and $h = 0.01a$.

Depending on structural parameters, this index is either pure imaginary or real, thereby representing the metal and insulator phases, respectively. When structural parameters are varied continuously, we observe that the change of refractive index from pure imaginary to real, or metal-to-insulator transition, occurs when the denominator passes zero, or when the gap size g_x exceeds the critical value g_t, which is determined by

$$\frac{h\pi}{g_t} - 2\ln\left(\frac{2\pi g_t}{d_x}\right) = \frac{\lambda^2 d_y^3}{4d_x b^4} - 3. \tag{20}$$

This is a condition for the phase transition with a critical lattice spacing. We point out that the same condition can be derived from the vanishing transmission, $T_{y,00} = 0$. In the transition condition in Equation (20), g_t is determined only implicitly. For convenience, we re-express the transition condition in terms of the critical frequency ω_t for given gap sizes g_{xy} such that

$$\omega_t \equiv \frac{\pi d_y c_0}{b^2}\sqrt{\frac{d_y}{2d_x}}\left(\frac{h\pi}{2g_x} - \ln\left(\frac{2g_x\pi}{d_x}\right) + \frac{3}{2}\right)^{-1/2} \tag{21}$$

where $\omega_t = 2\pi c_0/\lambda_t$, c_0 is the speed of light in a vacuum, and λ_t is the gap-size-dependent transition wavelength. Then, Equation (19) can be simplified in terms of transition frequency:

$$n_{eff} \approx \sqrt{\frac{8ad_y^2 c_0^2}{d_x b^3 h\pi}}\sqrt{\frac{1}{\omega_t^2 - \omega_0^2}}. \tag{22}$$

Note that Equation (22) is valid when $g_x, h \ll d_x, d_y < \lambda$. In the same manner, explicit calculation also shows that the effective impedance in Equation (16) can be approximated as

$$Z_{eff} \approx \sqrt{\frac{8ahb^5}{c_0^2\pi^3 d_x d_y^4}}\sqrt{\omega_t^2 - \omega^2}^{*}, \tag{23}$$

and effective permittivity and permeability of the metasurface by

$$\varepsilon_{eff}^{xx} \approx \frac{c_0^2\pi d_y^3}{hb^4}\frac{1}{\omega_t^2 - \omega^2},\ \mu_{eff}^{xx} \approx \frac{8ab}{\pi^2 d_x d_y}. \tag{24}$$

We note that the effective permittivity possesses a Lorentzian-type resonant behavior. We also note that similar expressions for ε_{eff}^{yy} and μ_{eff}^{yy} can be obtained with x, y interchanged.

Figure 3 shows the wavelength- and gap-dependent effective permittivity of the metasurface. One can clearly see that, for a fixed wavelength, the phase transition can be controlled by varying gap size at a deep subwavelength scale. We point out that our theory successfully resolves the extraordinarily high refractive index in [4]. We also note that the effective permeability is independent of gap size agreeing with the result in [22].

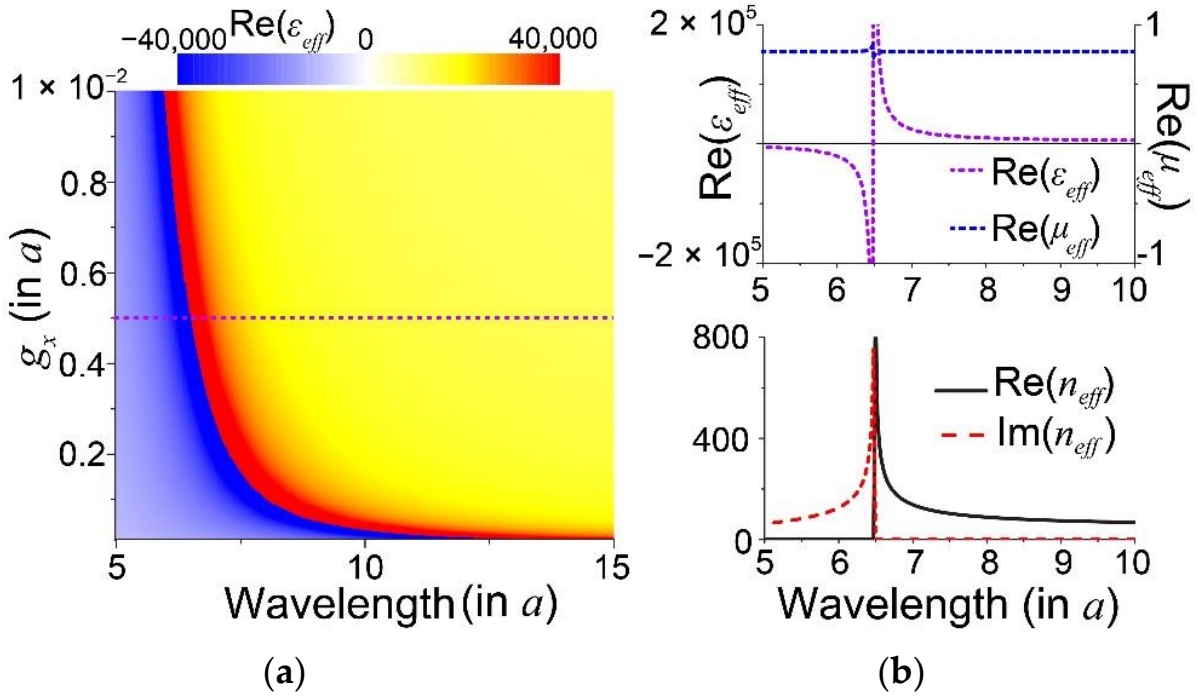

Figure 3. (**a**) Analytically calculated wavelength- and gap-dependent effective permittivity of a metasurface of $a = b$, $w = 0.01a$, $h = 0.01a$. (**b**) The upper panel shows a cross-cut spectrum of effective permittivity (purple) and permeability (blue) at $g_x = 0.005a$. The cut line is shown in (**a**) as a dotted line. The bottom panel shows corresponding effective refractive indices.

4. Discussion

4.1. The Origin of the Metal-to-Insulator Transition: Macroscopic Channel Competition

So far, we discussed the gap-size-dependent metal-to-insulator transition based on the far-field transmission and reflection coefficients. One of the main advantages of using the coupled-mode theory is that the theory provides the full descriptions of the electromagnetic field distribution near the metasurface, allowing understanding of how the transition is related to the macroscopic near-field features. Specifically, one can rewrite the far-field transmission coefficient in Equation (8) as

$$T_{y,00} = \left(\int_{c^{(1)}} dxdy + \int_{c^{(2)}} dxdy \right) \frac{E_{xII}(x,y)}{d_x d_y}. \tag{25}$$

We previously discussed that the transition condition can be also obtained by letting $T_{y,00} = 0$. This means that, from Equation (25), the phase transition occurs when the transmissions of the E_x fields in two channels cancel each other out. To be specific, we first evaluate the integral over the $c^{(1)}$ channel, averaging E_x on a unit lattice. This gives rise to

$$\overline{E_x^{(1)}} \equiv \int_{c^{(1)}} \frac{E_{xII}}{d_x d_y} dxdy|_{z=0} \approx \frac{2ab\omega^2}{\pi d_x d_y} \times \frac{\left(\omega^2 - \omega_t^2\right) - i\alpha}{\left(\omega^2 - \omega_t^2\right)^2 + \alpha^2}, \tag{26}$$

where $\alpha \equiv \pi d_y^3 \omega^2 / 2b^4 k_0 > 0$. Comparing with Equation (24), we find that the sign of $\mathrm{Re}\left(\overline{E_x^{(1)}}\right)$ is opposite to that of the effective permittivity and vanishes at the transition frequency, whereas $\mathrm{Im}\left(\overline{E_x^{(1)}}\right)$ does not vanish. For the second channel $c^{(2)}$, one can find that an explicit calculation yields the same trend except for the overall sign change. Therefore, the metal-to-insulator transition condition can be restated in terms of lattice-averaged electric field components by

$$\mathrm{Re}\left(\overline{E_x^{(1)}}\right) = \mathrm{Re}\left(\overline{E_x^{(2)}}\right) = 0, \ \mathrm{Im}\left(\overline{E_x^{(1)}}\right) + \mathrm{Im}\left(\overline{E_x^{(2)}}\right) = 0. \tag{27}$$

On the other hand, the magnetic field components in each channel can be written as $H_{yII}^{(1)} \approx 4Z_0^{-1} \sin(\pi y/b)/\pi$ and $H_{yII}^{(2)} \approx Z_0^{-1}$ with negligible imaginary. Consequently, the total energy flux through the metasurface, equivalent to the z-component of the time-averaged Poynting vector $\left\langle \vec{S} \right\rangle \equiv \mathrm{Re}\left(\vec{E} \times \vec{H}^*\right)/2$, can be simplified as $\langle S_z \rangle \approx \mathrm{Re}(E_x) H_y/2$. This gives rise to an intuitive criterion for the metal and insulator phases of a metasurface through

$$\begin{aligned} &\left\langle S_z^{(1)} \right\rangle > 0, \ \left\langle S_z^{(2)} \right\rangle < 0, \ \varepsilon_{eff} < 0 \text{ for metal,} \\ &\left\langle S_z^{(1)} \right\rangle < 0, \ \left\langle S_z^{(2)} \right\rangle > 0, \ \varepsilon_{eff} > 0 \text{ for insulator.} \end{aligned} \tag{28}$$

This is one of our main observations. The effective phase becomes metal when incident light transmits through the evanescent channel $c^{(1)}$; otherwise, it becomes insulator. This means that the effective phase follows the characteristic of the channel through which incident light passes. Therefore, the phase transition is a result of the competition between those light channels to admit the incident light.

4.2. Test of the Validity of the Effective Parameters

In order to check the validity of our theory, we examined light transmission through multilayered metasurfaces, as shown in Figure 4. The metasurfaces, samples 1 and 2, are made of rectangular rings as depicted in Figure 1 with $a = b$, $d_x = d_y = d$, and $g_x \neq g_y$. Sample 2 is the 90-degree rotated version of sample 1. Both samples 1 and 2 are designed to exhibit strongly anisotropic optical responses in x- and y-directions and to have opposite signs in the effective permittivities in a particular spectral range (the pink-colored regions in Figure 4). The spacing between each layer is kept as $d/2\pi$ to allow two neighboring metasurfaces to interact with each other via only zero-th order waves. Note that the momentum of the first-order diffracted wave is given by $\chi_{01} = \chi_{10} = \left(k_0^2 - (2\pi/d)^2\right)^{1/2}$. Therefore, for a deep subwavelength periodicity d, the longest penetration depth for the diffracted wave is approximately given by $\left(k_0^2 - (2\pi/d)^2\right)^{-1/2} \approx d/2\pi$. This spacing is required to use the same effective permittivities in both single- and multilayered systems.

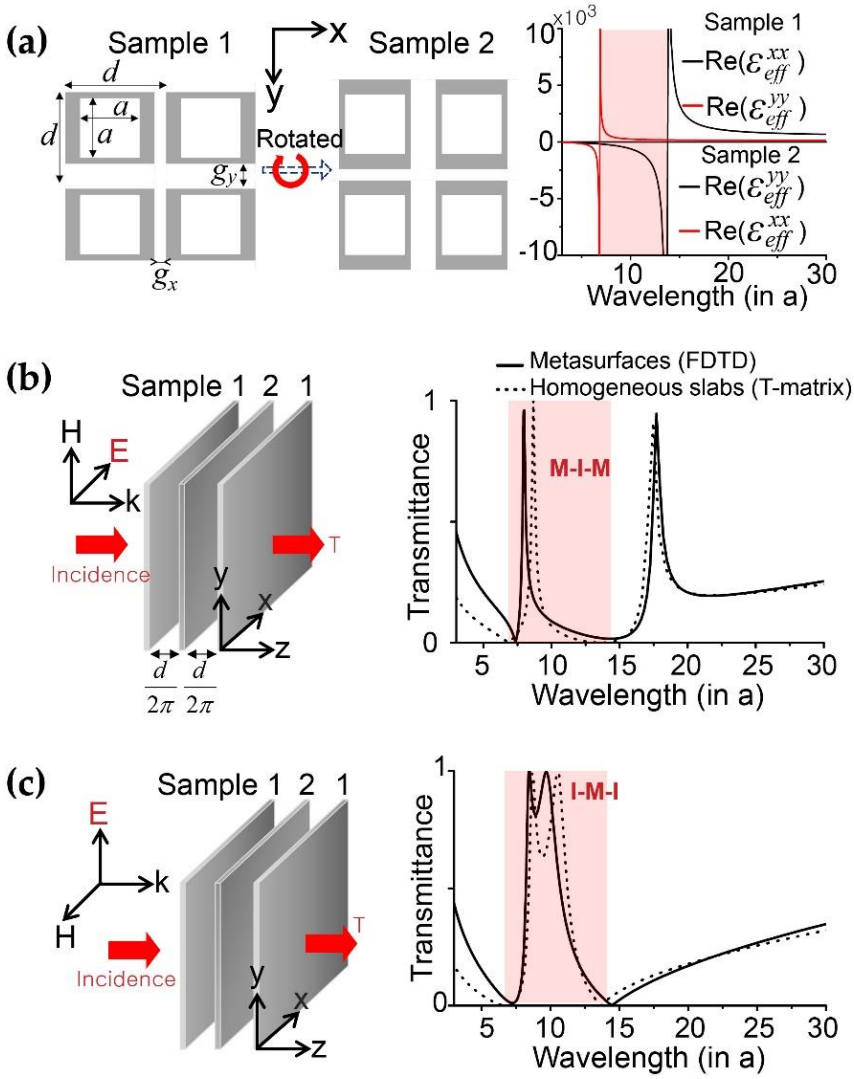

Figure 4. (**a**) Schematic of two metasurfaces, 1 and 2, and corresponding effective permittivities where $g_x = 0.0025a$, $g_y = 0.0188a$, $h = 0.03a$, and $d = 1.0375a$. (**b**) FDTD-calculated transmission spectrum (solid line) through the 1-2-1 layer with x-polarized incident light and (**c**) with y-polarized incident light. Dotted lines are the spectrum obtained from the transfer matrix scheme applied to multilayered homogeneous slabs possessing effective permittivities corresponding to (**a**).

Shown in Figure 4b,c are the transmission spectra of x- and y-polarized incident lights, respectively, through the 1-2-1 layered system. For the numerical calculations by implementing inhomogeneous 2D metasurfaces, we used the finite-difference time-domain (FDTD) method. In the colored spectral range, our system effectively becomes a metal–insulator–metal (M–I–M) or I–M–I multilayered system depending on the polarization. In Figure 4b, we can see a peak in the colored region that corresponds to resonant tunneling through two metallic barriers, and another peak at a longer wavelength that originates from the Fabry–Perot resonance. With an incident light rotated as shown in Figure 4c, two peaks appear in the colored regions. These peaks also correspond to resonant tunneling, which appear in negative-permittivity media as demonstrated in [23]. For comparison, we calculated the transmission spectra through multilayered homogeneous slabs possessing corresponding effective permittivities. We note that all transmission spectra are in good agreement.

5. Conclusions

In conclusion, we theoretically demonstrated metal-to-insulator transition in metasurfaces that can be controlled by the lattice spacing of the unit resonators. Through analytic calculations on the model metasurface, we rigorously defined the critical gap size g_t at which the transition occurs. Additionally, by seeking the macroscopic details of the electromagnetic waves in the proximity of the metasurface, we defined quantitative criteria for the phase transition. Our theory demonstrates that drastic changes in optical responses can emerge from the interactions between unit resonators, an observation that is essential for the engineering of metasurfaces with tightly coupled unit resonators for deformable, reconfigurable, and functionalized metamaterials aiming for ultra-high-sensitive optical responses and dynamic manipulation of their effective properties.

Author Contributions: Conceptualization, J.-H.K.; methodology, S.L. and J.-H.K.; investigation, S.L. and J.-H.K.; data curation, S.L. and J.-H.K.; writing—original draft preparation, S.L. and J.-H.K.; writing—review and editing, S.L. and J.-H.K.; supervision, J.-H.K. All authors have read and agreed to the published version of the manuscript.

Funding: This research was supported by a research grant from Kongju National University in 2020 and by a National Research Foundation of Korea (NRF) grant funded by the Korean government (MSIT) (grant nos. NRF-2020R1F1A1076886 and NRF-2021R1A2C2012617). S.L. was supported by an NRF grant funded by the Korean government (MSIT) (grant no. NRF-2020R1C1C1012138).

Institutional Review Board Statement: Not applicable.

Informed Consent Statement: Not applicable.

Data Availability Statement: Data are available from the corresponding author on request.

Conflicts of Interest: The authors declare no conflict of interest.

References

1. Zylbersztejn, A.; Mott, N.F. Metal-insulator transition in vanadium dioxide. *Phys. Rev. B* **1975**, *11*, 4383. [CrossRef]
2. Kibis, O.V. Metal-insulator transition in graphene induced by circularly polarized photons. *Phys. Rev. B Condens. Matter Mater. Phys.* **2010**, *81*, 165433. [CrossRef]
3. Seo, M.; Kyoung, J.; Park, H.; Koo, S.; Kim, H.S.; Bernien, H.; Kim, B.J.; Choe, J.H.; Ahn, Y.H.; Kim, H.T.; et al. Active terahertz nanoantennas based on VO2 phase transition. *Nano Lett.* **2010**, *10*, 2064–2068. [CrossRef]
4. Choi, M.; Lee, S.H.; Kim, Y.; Kang, S.B.; Shin, J.; Kwak, M.H.; Kang, K.Y.; Lee, Y.H.; Park, N.; Min, B. A terahertz metamaterial with unnaturally high refractive index. *Nature* **2011**, *470*, 369–373. [CrossRef] [PubMed]
5. Takano, K.; Shibuya, K.; Akiyama, K.; Nagashima, T.; Miyamaru, F.; Hangyo, M. A metal-to-insulator transition in cut-wire-grid metamaterials in the terahertz region. *J. Appl. Phys.* **2010**, *107*, 024907. [CrossRef]
6. Smith, D.R.; Schurig, D. Electromagnetic Wave Propagation in Media with Indefinite Permittivity and Permeability Tensors. *Phys. Rev. Lett.* **2003**, *90*, 077405. [CrossRef] [PubMed]
7. Lee, S.; Kim, W.T.; Kang, J.H.; Kang, B.J.; Rotermund, F.; Park, Q.H. Single-Layer Metasurfaces as Spectrally Tunable Terahertz Half- A nd Quarter-Waveplates. *ACS Appl. Mater. Interfaces* **2019**, *11*, 7655–7660. [CrossRef] [PubMed]
8. Luan, P.G. Effective electrodynamics theory for the hyperbolic metamaterial consisting of metal–dielectric layers. *Crystals* **2020**, *10*, 863. [CrossRef]
9. Biehs, S.A.; Tschikin, M.; Ben-Abdallah, P. Hyperbolic metamaterials as an analog of a blackbody in the near field. *Phys. Rev. Lett.* **2012**, *109*, 104301. [CrossRef] [PubMed]
10. Salandrino, A.; Engheta, N. Far-field subdiffraction optical microscopy using metamaterial crystals: Theory and simulations. *Phys. Rev. B Condens. Matter Mater. Phys.* **2006**, *74*, 075103. [CrossRef]
11. Slobozhanyuk, A.P.; Ginzburg, P.; Powell, D.A.; Iorsh, I.; Shalin, A.S.; Segovia, P.; Krasavin, A.V.; Wurtz, G.A.; Podolskiy, V.A.; Belov, P.A.; et al. Purcell effect in hyperbolic metamaterial resonators. *Phys. Rev. B Condens. Matter Mater. Phys.* **2015**, *92*, 195127. [CrossRef]
12. Maas, R.; Parsons, J.; Engheta, N.; Polman, A. Experimental realization of an epsilon-near-zero metamaterial at visible wavelengths. *Nat. Photonics* **2013**, *7*, 907–912. [CrossRef]
13. Decker, M.; Feth, N.; Soukoulis, C.M.; Linden, S.; Wegener, M. Retarded long-range interaction in split-ring-resonator square arrays. *Phys. Rev. B Condens. Matter Mater. Phys.* **2011**, *84*, 085416. [CrossRef]
14. Kang, J.; Lee, S.; Kang, B.J.; Kim, W.T.; Rotermund, F.; Park, Q.-H. Anomalous Wavelength Scaling of Tightly-Coupled Terahertz Metasurfaces. *ACS Appl. Mater. Interfaces* **2018**, *10*, 19331–19335. [CrossRef] [PubMed]

15. Yoo, S.J.; Park, Q.-H. Effective permittivity for resonant plasmonic nanoparticle systems via dressed polarizability. *Opt. Express* **2012**, *20*, 16480–16489. [CrossRef]
16. Kim, K.-H.; Jung, G.-H.; Lee, S.-J.; Park, H.-G.; Park, Q.-H. Ultrathin Capacitive Metasurfaces for Strong Electric Response. *Adv. Opt. Mater.* **2016**, *4*, 1501–1506. [CrossRef]
17. Kang, J.H.; Kim, D.S.; Park, Q.H. Local capacitor model for plasmonic electric field enhancement. *Phys. Rev. Lett.* **2009**, *102*, 093906. [CrossRef]
18. Seo, M.A.; Park, H.R.; Koo, S.M.; Park, D.J.; Kang, J.H.; Suwal, O.K.; Choi, S.S.; Planken, P.C.M.; Park, G.S.; Park, N.K.; et al. Terahertz field enhancement by a metallic nano slit operating beyond the skin-depth limit. *Nat. Photonics* **2009**, *3*, 152–156. [CrossRef]
19. Kang, J.-H.; Wang, S.; Shi, Z.; Zhao, W.; Yablonovitch, E.; Wang, F. Goos-Hänchen Shift and Even–Odd Peak Oscillations in Edge-Reflections of Surface Polaritons in Atomically Thin Crystals. *Nano Lett.* **2017**, *17*, 1768–1774. [CrossRef]
20. Kang, J.H.; Choe, J.-H.; Kim, D.-S.; Park, Q.-H. Substrate effect on aperture resonances in a thin metal film. *Opt. Express* **2009**, *17*, 15652–15658. [CrossRef]
21. Smith, D.R.; Vier, D.C.; Koschny, T.; Soukoulis, C.M. Electromagnetic parameter retrieval from inhomogeneous metamaterials. *Phys. Rev. E Stat. Nonlinear Soft Matter Phys.* **2005**, *71*, 036617. [CrossRef] [PubMed]
22. Pendry, J.B.; Martín-Moreno, L.; Garcia-Vidal, F.J. Mimicking surface plasmons with structured surfaces. *Science* **2004**, *305*, 847–848. [CrossRef] [PubMed]
23. Zhou, L.; Wen, W.; Chan, C.T.; Sheng, P. Electromagnetic-wave tunneling through negative-permittivity media with high magnetic fields. *Phys. Rev. Lett.* **2005**, *94*, 243905. [CrossRef]